Supplementary Information

1. Experimental information

1.1 Materials

All the materials, including graphitic C_3N_4 (GCN synthesized from urea annealing, ~500 nm nanoflakes, Zhongke Materials Co. Ltd, China) and Rhodamine B (RhB, Sigma-Aldrich) are commercially available and used as received.

1.2 GCN immobilization and flow cell assemblage

To prepare the sample, 0.1 mg of GCN was dispersed in 5 mL of ethanol and ultrasonicated for 30 minutes. A 0.5 mL aliquot of the upper layer of the dispersion was then deposited on a coverslip (24 mm in width and 50 mm in length) that had been preheated to 150°C. We carefully controlled the GCN particle distribution to achieve a homogeneous dispersion of approximately 5×10^3 particles per square millimeter. This optimal density ensures efficient high-throughput imaging while maintaining single-particle resolution, preventing both undersampling and particle overlapping. The sample was subsequently dried for 30 minutes at 80°C to immobilize the GCN particles on the coverslip surface. The GCN particles were subjected to a thermal process for 30 minutes at 80°C in a vacuum oven to enhance their adhesion to the glass substrate. This critical step ensures particle stability during extended imaging sessions of over 10 hours and withstands the flow forces in our microfluidic setup.

The coverslip bearing the GCN particles was then sealed in a flow cell with a channel dimension of 5 mm in width and 20 mm in length.[1] The flow cell is integral to our experimental design, serving two crucial functions. Firstly, it enables precise control of RhB concentration for titration experiments while maintaining fixed GCN particle positions, allowing us to observe concentration-dependent adsorption behavior on individual particles. Secondly, it provides a dynamic environment that mimics real-world continuous flow systems, enhancing the relevance of our findings to practical water treatment applications. To facilitate sample localization during scanning electron microscopy (SEM) after optical fluorescence imaging, the area of interest on the coverslip was demarcated by several shallow scratches, which served as fiducial markers.

1.3 Imaging set-up

Microscopic experiment experiments were conducted using an Olympus IX73 inverted microscope equipped with x60, UPLSAPO60XW, NA1.20, WD0.28 mm objective lens. Movies were recorded by Andor Sona 2.0B-11 sCMOS at the frame rate of 15 Hz with an exposure time of 50 ms, capturing 10000 frames in a movie. The excitation light was generated

by 532 nm Thorlabs LED. The excitation beam is filtered using a bandpass fluorescent filter 520 nm/70 nm 93T d25 filter, reflected by a 552 nm, 25.2x35.6 mm dichroic mirror. The emission light was collected by the same objective lens and passed through the emission filter as 585 nm/40 nm 93T d25.

1.4 Microscopic RhB concentration titration and bulk titration

For microscopic concentration titration, the RhB solution in water with different concentration from dilute to concentrate was pumped into the flow cell chip at a rate of 0.025 mL min^{-1} for 30 min before the fluorescence movie recording. The concentration series included 0, 0.048, 0.104, 0.209, 0.313, 0.418, 0.668, 1.04, 1.46, 2.09, 3.13, 4.18, 6.68, 10.4, 14.6, 20.9, 31.3, 41.8, 66.8, 104, 146, and 417 nM.

Bulk titration data were obtained by measuring the UV-vis absorbance of the solution. Typically, 10 mg of GCN powder was dispersed in 5 mL of water containing RhB and ultrasonicated for 5 minutes, followed by stirring for 30 minutes. The sample was then centrifuged at 7000 rpm for 5 minutes, and the clear liquid layer was filtered through a 0.22 μm hydrophilic membrane. The filtered solution was transferred into a 3 mL cuvette with a standard path length of 10 mm for UV-vis measurements. The UV-vis characterization provided absorbance data for light wavelengths ranging from 400 to 700 nm, using a Xe lamp with a sampling interval of 1 nm and a dwelling time of 0.2 s. The absorbance values were converted to concentration values using the Beer–Lambert law and a standard RhB absorbance-concentration curve. The standard curve was obtained by measuring the absorbance of a series of RhB standard solutions with concentrations ranging from 0.1 to 10 mg L^{-1}. The Raman spectrometry of particles is detected on a HORIBA LabRAM confocal Raman microscope with 100x objective, samples are excited using 20 mW 514 nm laser.

1.5 SEM imaging

SEM images were acquired using a Zeiss Supra 40 or Sigma 300 microscope operating at an accelerating voltage of 5.00 kV. Following the *in situ* fluorescence imaging, the flow cell was carefully disassembled, and the optical imaging area (including coverslip substrate) was excised, dried, and mounted on a Cu stage. The sample was then sputter-coated with Au for 60 seconds using a magnetic sputtering system with a target current of 30 mA to enhance conductivity and minimize charging effects during SEM imaging.

1.6 Fluorescence image processing

The fluorescence movies were analyzed using a home-written MATLAB program, iQPALM (image based quantitative photo-activated localization microscopy), which have been reported in our previous study.[2] To prevent the bias introduced by the photoluminescence of GCN, the average photoluminescence of GCN particles was calculated from the fluorescence movies recorded without RhB and was subtracted from the other fluorescence images.

Given the peak emission of RhB at $\lambda_{RhB} = 582$ nm, and the objective numeric aperture (NA) at 1.2, the diffraction-limited width of two-dimensional Gaussian point spread function (PSF), defined as the half width at half maximum, *FWHM*, should be approximately:

$$FWHM = \frac{0.61 \lambda_{RhB}}{NA} = 295.3 \quad nm$$

The 2D gaussian standard deviation $\sigma_{x,y}$ is theoretically:

$$\sigma_{xy} = \frac{FWHM}{2\sqrt{2\ln 2}} = 125.6 \quad nm$$

In which the 2D Gaussian PSF is:

$$I(x,y) = C_1 \exp\left(-\frac{(x-x_0)^2}{2\sigma_x^2} - \frac{(y-y_0)^2}{2\sigma_y^2}\right) + C_2$$

The $I(x,y)$ is the sCMOS pixel intensity counts, x_0, y_0 are the PSF centroid position, C_1, C_2 are the amplitude and background of the PSF, respectively.

PSF fitting shows the PSF intensity by total counts, which is calculated to the true photon counts for sCMOS as:

$$N = \frac{G \times ads}{QE}$$

Herein, QE is the quantum efficiency of the detector (95% for ours), G is the sensitivity of detector, informing the electron number per digital count ($G = 1.82$ for our set-up using high dynamic range mode).

The distribution of PSF intensities in Figure 1d matches the gamma distribution, of which the probability distribution function (PDF) formula and mean value is:

$$f(N) = \frac{N^{k-1} e^{-N/\theta}}{\Gamma(N)\theta^k}, \hat{N} = \theta k$$

For $\theta = 255$, $k = 378$, the mean intensity of PSF in photon number is $\hat{N} = 964$.

The localization error (Err_i, i = x or y) of the product molecule centroid position was estimated according to reference:

$$Err_i = \sqrt{\frac{\sigma_i^2}{N} + \frac{a_i^2}{12N} + \frac{8\pi\sigma_i^2 b^2}{a_i^2 N^2}}$$

where a_i is the pixel size; b is the background noise. For dataset in Figure 1c, the mean value $\hat{b}$ is calculated as 2.95 photons (matches the device readout noise of 2.6 photons verified by producer's performance datasheet). Given the pixel size of 187.3 nm, the Err_i is estimated to be 13.8 nm.

1.7 Autocorrelation

The autocorrelation function is defined as:

$$\rho(Lag) = \frac{\sum_{n=1}^{N-Lag} (t_n - \hat{t})(t_{Lag+n} - \hat{t})}{N\sigma_t^2}$$

Herein, ρ is the normalized autocorrelation coefficient. N is the number of t_{on} values in a sample series, σ_t and $\hat{t}$ are the sample variance and mean of the t_{on} series, respectively. *Lag* is defined as the lagging counts between two t_{on} values in the sample series.

1.8 Simulation

Density functional theory (DFT) calculations were performed with the "Vienna ab initio simulation package" (VASP 6.3.2) to investigate the interaction between pollutants/PMS and catalysts. Supercell (3 × 3 × 1) of C_3N_4 that includes 54 C atoms and 72 N atoms was repeated periodically on the x−y plane, and a vacuum region of 20 Å was applied along the z-direction to avoid the interactions between repeating slabs. The generalized gradient approximation with the functional of Perdew−Burke−Ernzerhof (PBE) functional was utilized for all geometric optimizations. The PBE + D3 method with the Becke-Jonson damping van der Waals correction was employed.[3,4] Plane-wave cutoff energy was set to 400 eV and Monkhorst-Pack K points were set to 1 × 1 × 1. The convergence criteria for structure optimization were set to: (1) energy tolerance of 1.0×10^{-4} eV/atom, (2) maximum force tolerance of 0.03 eV/Å.

2. Supplementary Figures

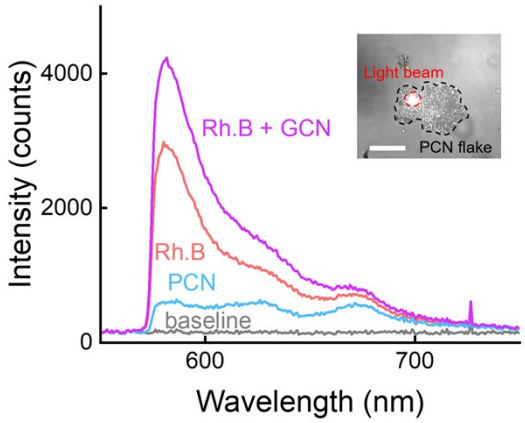

Figure S1. Local fluorescence spectrums of a GCN chunk with (purple) or without (blue) Rh.B. Subtraction of the spectrum provides the fluorescence spectrum of absorbed Rh.B molecules (red) on GCN. Gray line shows the negligible baseline without GCN. The bright field optical image (inset, scale bar = 5 μm) shows the location of the GCN particle and focused beam that excites the dye molecules.

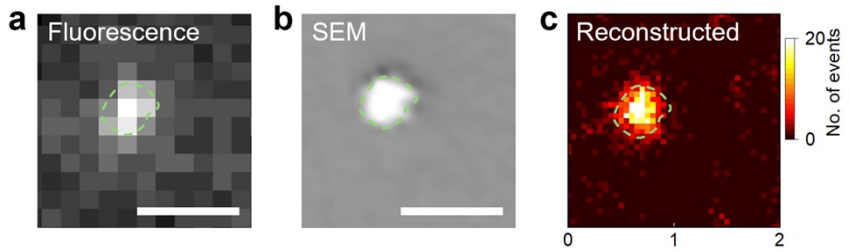

Figure S2. a) Wide-field fluorescence imaging under 1 second exposure, b) SEM image, and c) PAINT image reconstructed by 2D histogram (bin size: 50 nm) of fluorescent events of the same single PCN nanoflake, scale bar = 1 μm.

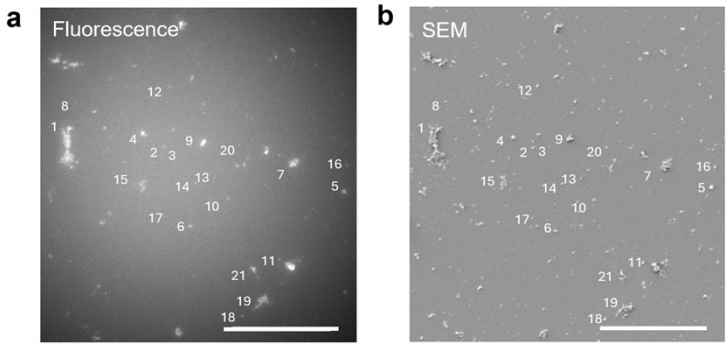

Figure S3. a) the fluorescence image and b) SEM images of more than 20 GCN particles in the same field of view, scale bar = 50 μm.

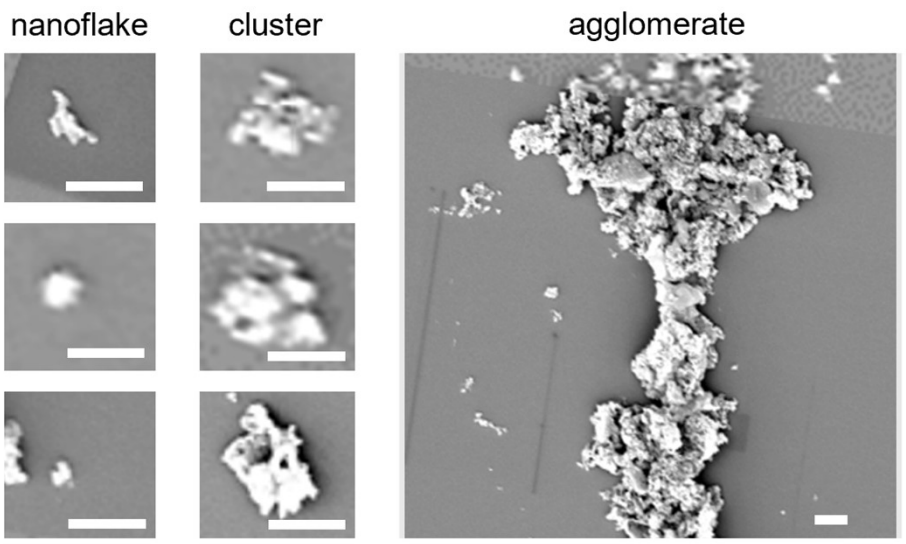

Figure S4. SEM images of GCN particles. GCN are classified in nanoflakes (mean diameter < 1 μm), cluster (1 μm < mean diameter < 5 μm), and large agglomerate on coverslip. Scale bar = 1 μm.

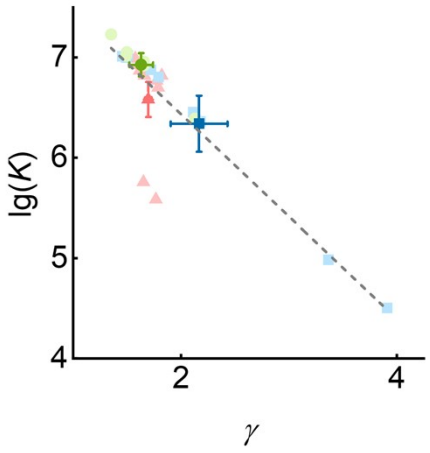

Figure S5. 2D distribution of thermodynamics for particles with different morphologies including nanoflake, cluster, and agglomerate in lg(K) and γ dimensions.

References

1. X. Mao, C. Liu, M. Hesari, N. Zou and P. Chen, *Nature Chemistry*, 2019, **11**, 687-694.
2. X. Mao and P. Chen, *Nature Materials*, 2022, **21**, 331-337.
3. S. Grimme, J. Antony, S. Ehrlich and H. Krieg, *The Journal of Chemical Physics*, 2010, **132**, 154104.
4. S. Grimme, S. Ehrlich and L. Goerigk, *Journal of Computational Chemistry*, 2011, **32**, 1456-1465.